Journal of Power Sources 247 (2014) 117–126

Contents lists available at ScienceDirect

Journal of Power Sources

journal homepage: www.elsevier.com/locate/jpowsour

Synthesis and electrochemical performance of LiV_3O_8/polythiophene composite as cathode materials for lithium ion batteries

Haipeng Guo, Li Liu*, Hongbo Shu, Xiukang Yang, Zhenhua Yang, Meng Zhou, Jinli Tan, Zichao Yan, Hai Hu*, Xianyou Wang

School of Chemistry, Key Laboratory of Environmentally Friendly Chemistry and Applications of Ministry of Education, Xiangtan University, Xiangtan 411105, China

HIGHLIGHTS

- The LiV_3O_8/polythiophene composite has been firstly synthesized and investigated.
- LiV_3O_8/polythiophene composite shows the excellent electrochemical performance.
- Polythiophene coating improve electrochemical performance of LiV_3O_8 significantly.

ARTICLE INFO

Article history:
Received 21 May 2013
Received in revised form
6 August 2013
Accepted 20 August 2013
Available online 3 September 2013

Keywords:
Lithium ion batteries
Lithium vanadium oxide
Polythiophene
Composites

ABSTRACT

LiV_3O_8/polythiophene (LiV_3O_8/PTh) composite has been chemically synthesized via an in-situ oxidative polymerization method. The structure and morphology of the samples have been characterized by X-ray diffraction (XRD), Fourier transform infrared spectroscopy (FTIR), scanning electron microscopy (SEM) and high-resolution transmission electron microscopy (HRTEM). LiV_3O_8/PTh composite shows a single phase in the XRD pattern, but the existence of PTh has been confirmed by FTIR spectra. HRTEM images show that an uniform PTh layer with a thickness of 3–5 nm covered on the surface of LiV_3O_8. Electrochemical performance of samples has been characterized by the charge/discharge test, cyclic voltammetry (CV), electrochemical impedance spectroscopic studies (EIS) and galvanostatic intermittent titration technique (GITT). The LiV_3O_8/PTh composite exhibits much better electrochemical performance than bare LiV_3O_8. The initial discharge capacities of 15 wt.% LiV_3O_8/PTh composite are 213.3 and 200.3 mAh g^{-1} with almost no capacity retention after 50 cycles at current densities of 300 and 900 mA g^{-1}, respectively. PTh could enhance electronic conductivity, decrease the charge transfer resistance, increase the lithium diffusion coefficient, and thus improve cycling performance of LiV_3O_8. All these results demonstrate that the LiV_3O_8/PTh composite has a promising application as cathode material for lithium ion batteries.

1. Introduction

With the rapid development of portable devices and hybrid electric vehicles, lithium ion batteries (LIBs) are widely considered to be the most promising electrochemical energy storage and transfer systems [1,2]. Although the current LIBs exhibit superior energy density, cycle stability and rate capability in comparison with other rechargeable batteries, such as silver–zinc and nickel–metal-hydride, their electrochemical performance have scarcely been improved, because of the limited theoretical capacity for these cathode materials ($LiCoO_2$, $LiMn_2O_4$, and $LiFePO_4$) [3]. Therefore, developing novel cathode materials are significant and these researches have been carried out extensively in recent years.

The lithium vanadium oxide (LiV_3O_8) is well-known as a promising cathode material for LIBs due to its high-specific capacity, good structural stability, low cost and good safety features [4–6]. It is known to all that the preparation methods as well as the material's morphology can strongly influence the electrochemical performance of LiV_3O_8 electrode, in aspects such as charge–discharge capacity, rate capacity, cycling stability, etc [7,8]. Up to now, nanoscale and well-ordered structures with various morphologies of LiV_3O_8 materials have also been studied extensively, for instance, nanorods [9], nanosheets [10], and nanotubes [11]. The nanomaterials provide short diffusion pathways for

* Corresponding authors. Tel.: +86 731 58292206; fax: +86 731 58292477.
E-mail addresses: liulili1203@126.com (L. Liu), huhai29@126.com (H. Hu).

0378-7753/$ – see front matter © 2013 Elsevier B.V. All rights reserved.
http://dx.doi.org/10.1016/j.jpowsour.2013.08.078

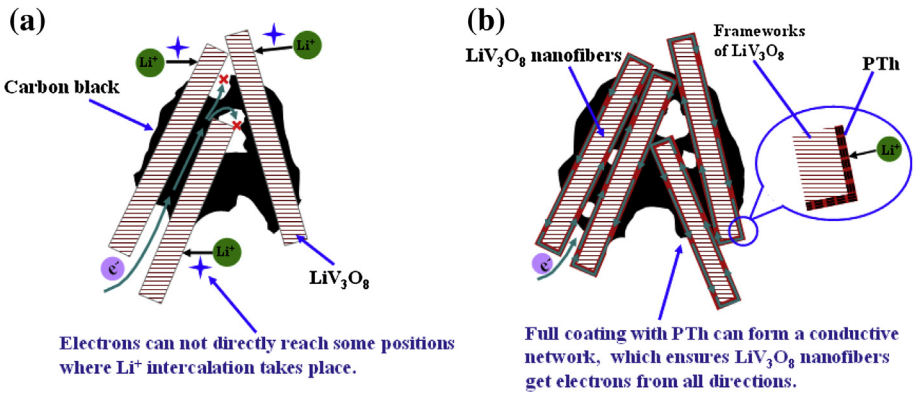

Fig. 1. (a) Electron-transfer pathway for LiV_3O_8 only with carbon black as conductive additives. (b) Designed ideal structure for LiV_3O_8 nanofibers with a complete polythiophene coating.

lithium ion insertion and extraction reactions, together with high specific surface areas, which can increase the contact between the active material and the electrolyte [12]. However, because of the phase transformation during cycling and dissolution of small quantity of LiV_3O_8 in the electrolyte, bare LiV_3O_8 exhibits poor rate capability and serious capacity fade during cycling, which restricts its application in rechargeable LIBs [13]. Therefore, many other strategies, such as structural/morphological modification by coating, have been suggested to further enhance the electrochemical performance of LiV_3O_8.

As has been reported in previous publications, coating is an effective method to improve the electrochemical performance of LiV_3O_8 [14–16]. The coating layers are able to enhance the electronic conductivity, inhibiting the phase transition, increasing structural stability, decreasing active material dissolution, which consequently leads to a remarkable improvement in reversible capacity, rate capability, cycle stability etc [17,18]. For example, Jiao et al. have demonstrated that 1 wt.% $AlPO_4$ nanowires coating effectively improved the cycling performance of LiV_3O_8 [14]. Idris et al. have reported that LiV_3O_8/carbon composite revealed enhanced rate capability [15]. Tian et al. have shown that the rate capability and cycle stability of LiV_3O_8 are improved by $Co_{0.58}Ni_{0.42}$ oxide nanoneedles coating [19].

More recently, the use of conducting polymer and vanadium oxide composite materials as electrodes is of great interest to improve the capacity, cycle stability and conductivity [20–23]. Different from other coating materials ($AlPO_4$ [14], Carbon [15], ZnO [16], $Co_{0.58}Ni_{0.42}$ [19]), conductive polymers can not only suppress the dissolution of active materials into the $LiPF_6$ electrolyte and improve the electrical conductivity of LiV_3O_8 significantly, but also participate electrochemical reaction during cycling and contribute to the specific capacity of the composites, which make them to be attractive additive materials for LIBs. To date, vanadium-based materials combined with polymers, such as LiV_3O_8/polypyrrole [8], LiV_3O_8/polyaniline [24], V_2O_5/polyaniline [22], V_2O_5/polypyrrole [23] and $Li_3V_2(PO_4)_3$/polyaniline [25] have been synthesized and showed improved cycling performance in LIBs. polythiophene (PTh) is a promising conducting polymer, a coating of PTh on the particles would increase the electronic conductivity of active material. Moreover, PTh also has electrochemical activity and contributes to the specific capacity of the composites [26]. Compared with polypyrrole and polyaniline, PTh has a higher conductivity and better coulombic efficiency [27]. These advantages make PTh more suitable as the coating material to improve the electrochemical properties of LiV_3O_8. However, to the best of our knowledge, though many researches about LiV_3O_8/polymer have been reported, there're few reports about LiV_3O_8/PTh.

Hence, we designed and demonstrated a facile method to fabricate LiV_3O_8/PTh in this study. The scheme of this study can be illustrated by Fig. 1. As shown in Fig. 1a, during the intercalation process, the electrons cannot reach all the positions where lithium ion intercalation takes place, thus results in polarization of the electrode. However, full coating with conducting polymer can form a conductive network, which ensures LiV_3O_8 nanofibers get electrons from all directions, consequently alleviates this polarization phenomenon (Fig. 1b). This method may provide a possible polymer-coating synthesis route that can be extended to many other materials. We focus on discussing the electrochemical performance of LiV_3O_8/PTh as cathode materials for LIBs and simultaneously try to probe the specific interactions between the PTh and LiV_3O_8, and how these interactions contribute to enhance the properties of LiV_3O_8.

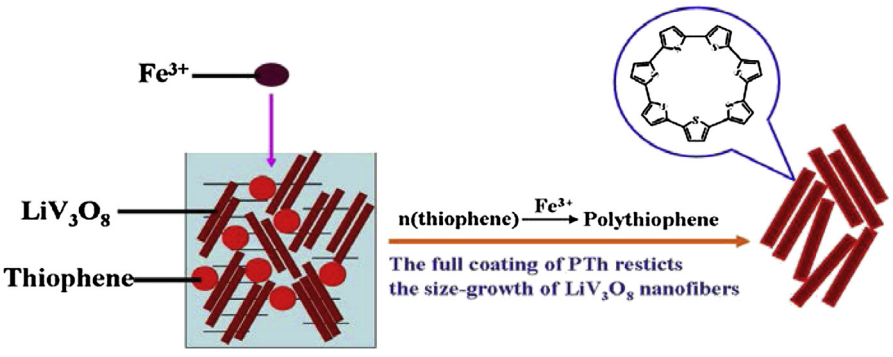

Fig. 2. Preparation processes of polythiophene-LiV_3O_8 composite including an in-situ polymerization reaction.

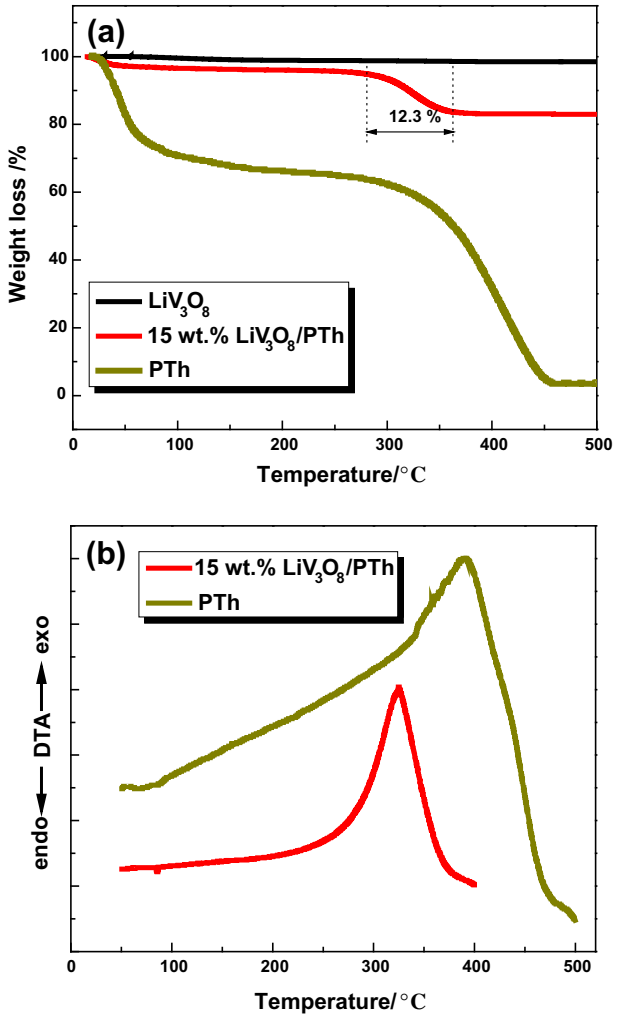

Fig. 3. (a) TGA curves of the PTh power, the bare LiV_3O_8 and 15 wt.% LiV_3O_8/PTh composite. (b) DTA curves of PTh power and 15 wt.% LiV_3O_8/PTh composite.

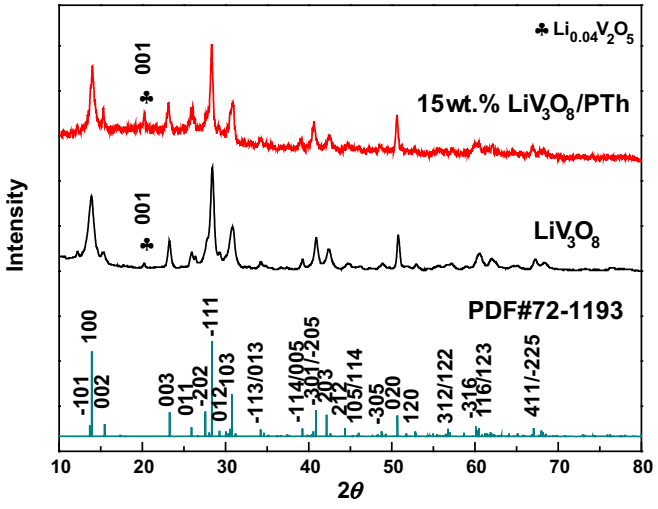

Fig. 4. XRD patterns of standard LiV_3O_8 (PDF: 72-1193), LiV_3O_8 and 15 wt.% LiV_3O_8/PTh composite.

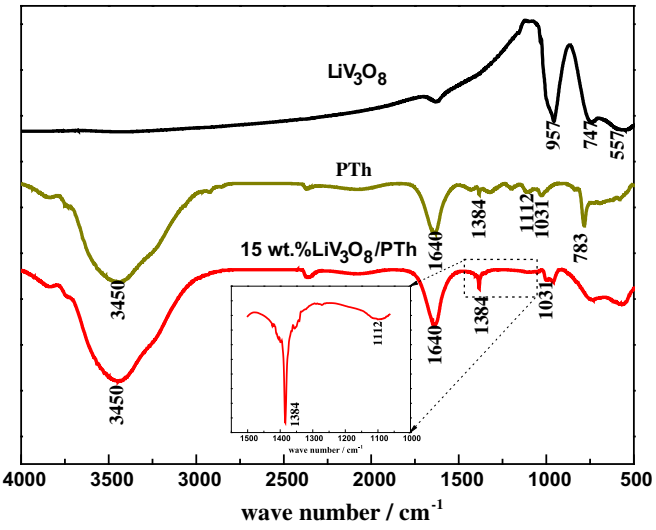

Fig. 5. FT–IR spectra measured on the KBr-diluted pellets of PTh, LiV_3O_8, and 15 wt.% LiV_3O_8/PTh composite.

2. Experimental

2.1. Preparation of cathode materials

LiV_3O_8 was synthesized by a classic peroxide sol–gel method [6]. Ten percent (v/v) peroxide solution was slowly added to a reaction vessel with a certain amount of V_2O_5, and the obtained solution was vigorously stirred for 2 h at room temperature to get a clear orange solution. Then, stoichiometric amounts of LiOH solution were added to the above orange solution with vigorous stirring. The resulting solution was maintained at 80–90 °C under stirring until Red-brown viscous gel was formed. The gel was dried in a vacuum oven at 120 °C for 24 h and then put into a tube oven for calcination at 300 °C for 16 h in air. Lastly, products were cooled and ground to fine polycrystalline reddish brown powders.

LiV_3O_8/PTh composite was synthesized by an in-situ chemical oxidative polymerization method (shown in Fig. 2). LiV_3O_8 was dispersed into 50 mL $CHCl_3$ solutions, forming LiV_3O_8 and $CHCl_3$ suspension. The suspension was magnetically stirred at 0 °C for 30 min. Afterward, the thiophene monomer (15 wt.%) was injected into the suspension, then 50 mL $FeCl_3$ (4:1 m m^{-1} $FeCl_3$/thiophene) solution was added dropwise to the suspension. The suspension was kept stirring at 0 °C for 6 h. Afterward, thiophene was polymerized in-situ on the surface of LiV_3O_8 to form a red–brown polythiophene shell that can both effectively restrict the aggregation of LiV_3O_8 particles and improve the electrical conductivity. After polymerization, the final LiV_3O_8/PTh product was filtered, washed with deionized water and ethanol alternately for several times. Finally, the red-brown mass was dried at 80 °C for 12 h in an oven to obtain the 15 wt.% LiV_3O_8/PTh powder. The preparation of other LiV_3O_8/PTh composite (10 and 20 wt.%) is similar to the above process except for the amounts of the thiophene monomer 10 and 20 wt.%, respectively.

2.2. Materials characterization and electrochemical measurements

The amount of polythiophene in LiV_3O_8/PTh composite was determined by thermogravimetric analysis (TGA) and differential thermal analysis (DTA). Thermogravimetric analysis was carried out in a thermogravimetric–differential thermo analyzer (Standard Type High temp. Type, Rigaku) in air and the samples were heated from room temperature to 500 °C at a slow scan rate of 5 °C min^{-1}.

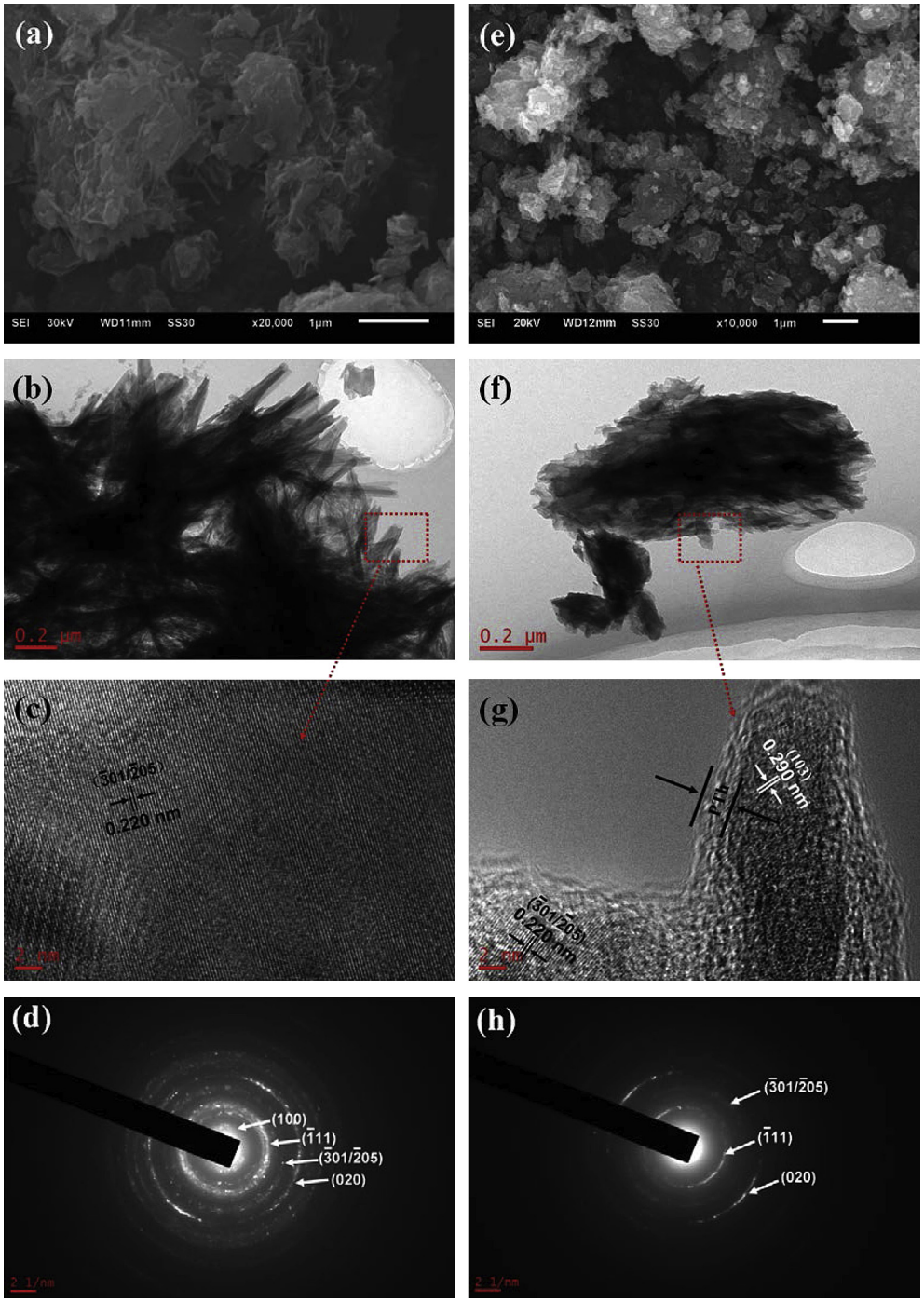

Fig. 6. SEM (a), TEM (b), HRTEM (c) and SAED (d) images of bare LiV_3O_8, SEM (e), TEM (f), HRTEM (g) and SAED (h) images of 15 wt.% LiV_3O_8/PTh composite.

The structures of synthesized samples were characterized by X-ray diffraction and FT–IR spectra. X-ray powder diffraction data were obtained using a Rigaku D/MAX-2500 powder diffractometer with a graphite monochromatic and Cu Kα radiation ($\lambda = 0.15418$ nm) in the 2θ range of 10–80°. FT–IR spectra were recorded with Perkin–Elmer Spectrum one FT–IR spectrophotometer using KBr pellets in the region 4000–400 cm^{-1}.

Scanning electron microscope (SEM) images of the samples were collected using a JEOL JSM-6610 scanning electron microscope, which were used to observe the particle morphology, particle size and particle size distribution. High-resolution transmission electron microscopy (HRTEM) and selected-area electron diffraction (SAED) measurements were carried out using a JEOL JEM-2100F transmission electron microscope at an acceleration voltage of 200 kV.

The cathodes for lithium cells were fabricated by mixing the cathode material, carbon black, and Polyvinylidene fluoride (PVDF) binder with a weight ratio of 85:10:5 in N-methyl pyrrolidinone, which were then pasted on an aluminum foil followed by drying under vacuum at 110 °C for 12 h. The testing cells were assembled with the cathodes thus fabricated, metallic lithium anode, Celgard 2300 film separator and 1 M $LiPF_6$ in 1:1 ethylene carbonate (EC)/dimethyl carbonate (DMC) electrolyte. The assembly of the testing cells was carried out in an argon-filled glove box, where water and

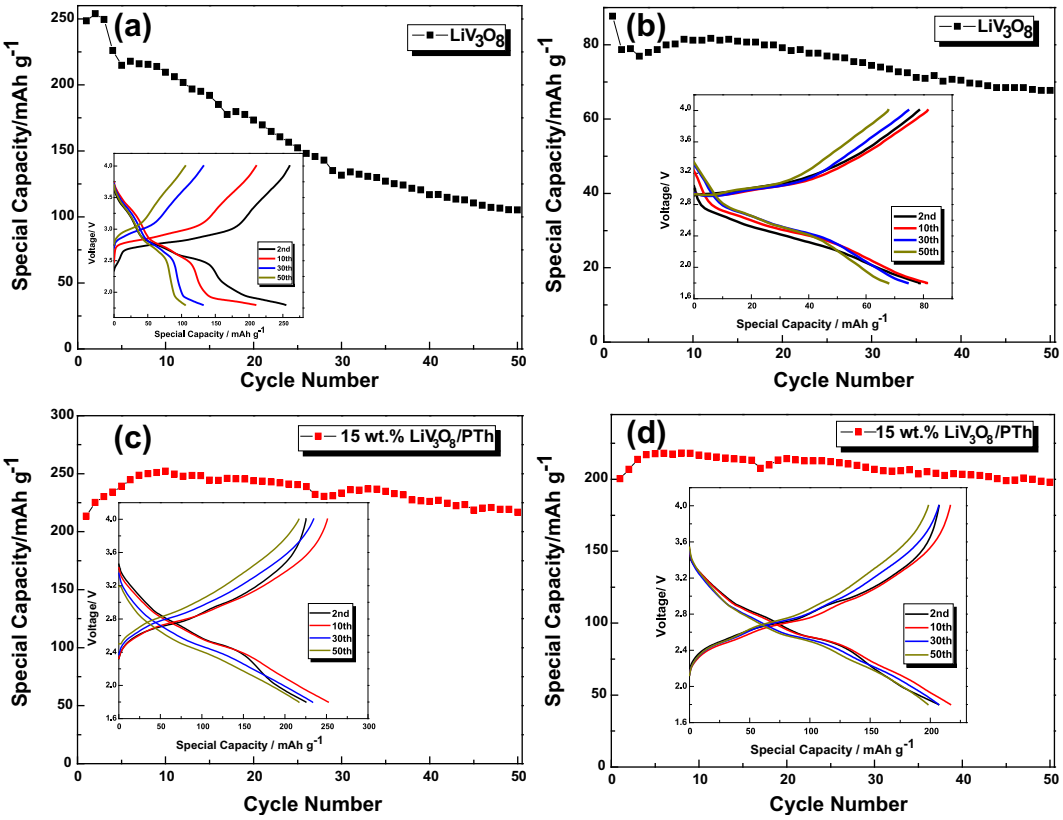

Fig. 7. Discharge capacity versus cycle number and discharge/charge profiles (insets) for the (a) LiV_3O_8 at a current density of 300 mA g^{-1} (1 C), (b) LiV_3O_8 at high current density of 900 mA g^{-1} (3 C), (c) 15 wt.% LiV_3O_8/PTh composite at a current density of 300 mA g^{-1} (1 C), and (d) 15 wt.% LiV_3O_8/PTh composite at high current density of 900 mA g^{-1} (3 C) in the range of 1.8–4.0 V (vs. Li^+/Li).

oxygen concentration were kept less than 5 ppm. The discharge–charge cycle tests were run at different current densities of 1 C and 3 C (300 mA g^{-1} was assumed to be 1 C rate) between 4.0 and 1.8 V. All the tests were performed at room temperature.

Cyclic voltammetry (CV) tests and EIS experiments were performed on a Zahner Zennium electrochemical workstation. CV tests were carried out at a scan rate of 1 mV s^{-1} on the potential interval 1.8–4.0 V (vs. Li^+/Li). The ac perturbation signal was ±5 mV and the frequency range was from 100 mHz to 100 KHz. Galvanostatic intermittent titration technique (GITT) was employed at a pulse of 0.01 C for 10 min and with 60 min interruption between each pulse.

3. Results and discussion

3.1. Characterization of LiV_3O_8/PTh composite

To estimate the amount of polythiophene in the 15 wt.% LiV_3O_8/PTh composite, thermogravimetric (TGA)-differential thermal (DTA) analyses were carried out in an air atmosphere. Fig. 3a shows the TGA analysis curves of the 15 wt.% LiV_3O_8/PTh composite along with those of bare LiV_3O_8 and PTh. It can be found that there is no weight loss for bare LiV_3O_8 until 500 °C, while PTh begins to decompose around 280 °C and completely disintegrates at 460 °C. Therefore, for the 15 wt.% LiV_3O_8/PTh composite, the main loss from 280 to 500 °C is assigned to the degradation of PTh, and the approximate weight contents of polythiophene in the composite are 12.3 wt.%. The amount of polythiophene in 10 wt.% PTh–LiV_3O_8 composite and 20 wt.% PTh–LiV_3O_8 composite are 8.2 wt.% and 18.3 wt.%, respectively (see Fig. S1 in Supporting Information). Fig. 3b shows the DTA thermograms, which measure the thermal transitions, for PTh power and 15 wt.% LiV_3O_8/PTh composite. All the samples exhibit exothermic transitions are peaking between 250 and 500 °C, which was attributed to the degradation of the polythiophene [28], and the results are consistent with the TGA curves.

The X-ray diffraction (XRD) measurement has been used to study the phase structure of the sample. Fig. 4 shows XRD patterns of the LiV_3O_8 and the 15 wt.% LiV_3O_8/PTh composite. Both samples show good crystal structure. Almost all of the diffractive peaks are well attributed to the monoclinic LiV_3O_8 structure with the space group $P21/m$ (JCPDS: 72-1193). The 15 wt.% LiV_3O_8/PTh composite also can be attributed to LiV_3O_8 structure well, and the PTh phase is not observed in this pattern. Besides, it is noted that a redundant diffraction peak corresponding to (001) diffraction direction of $Li_{0.04}V_2O_5$ appears in LiV_3O_8 and 15 wt.% LiV_3O_8/PTh samples, indicating that a small part of the raw material did not react completely during the synthesis process. It is known that $Li_{0.04}V_2O_5$ shows a much higher lithium ion diffusion coefficient than LiV_3O_8 and also possesses good electrochemical properties [29,30]. So this impure phase will not influence the electrochemical performance of LiV_3O_8 and 15 wt.% LiV_3O_8/PTh. The XRD patterns of 10 wt.% LiV_3O_8/PTh composite and 20 wt.% LiV_3O_8/PTh composite (Fig. S2 in Supporting Information) are similar to 15 wt.% LiV_3O_8/PTh in Fig. 4.

FT–IR analysis was conducted to confirm the existence of PTh in the composite. FT–IR spectra of LiV_3O_8, PTh and 15 wt.% LiV_3O_8/PTh composite are shown in Fig. 5. The FT–IR spectrum of bare LiV_3O_8 shows the characteristic absorption bands of the V–O–V and V=O vibrations observed at approximately 957, 747 and 557 cm^{-1} [31–33]. The band around 957 cm^{-1} is attributed to V=O stretching vibration [31]. The band around 747 cm^{-1} is attributed to the symmetric V–O–V stretching vibration [32,33]. And the band around 557 cm^{-1} is attributed to the asymmetric V–O–V stretching

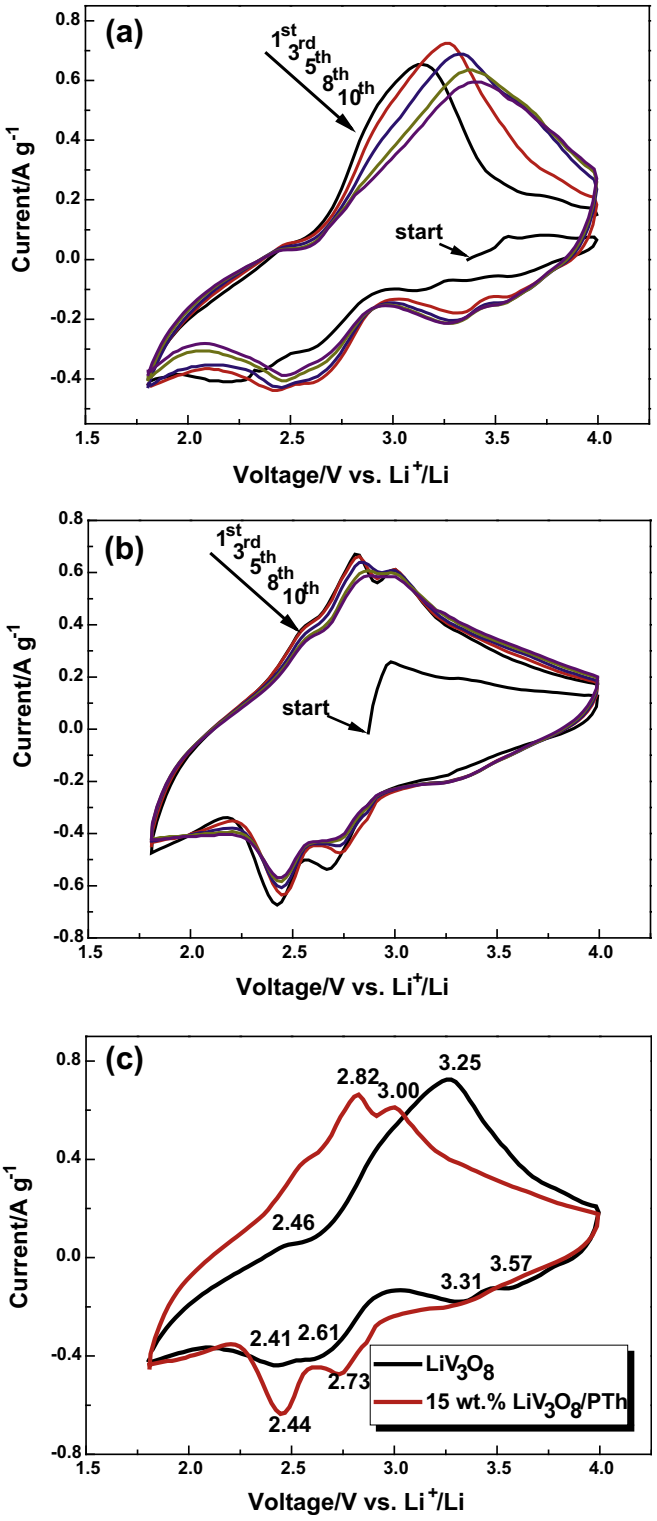

Fig. 8. Cyclic voltammograms of LiV_3O_8 (a), 15 wt.% LiV_3O_8/PTh composite (b), the third CV cycle of LiV_3O_8 and 15 wt.% LiV_3O_8/PTh (c). (Scan rate is 1 mV s^{-1}).

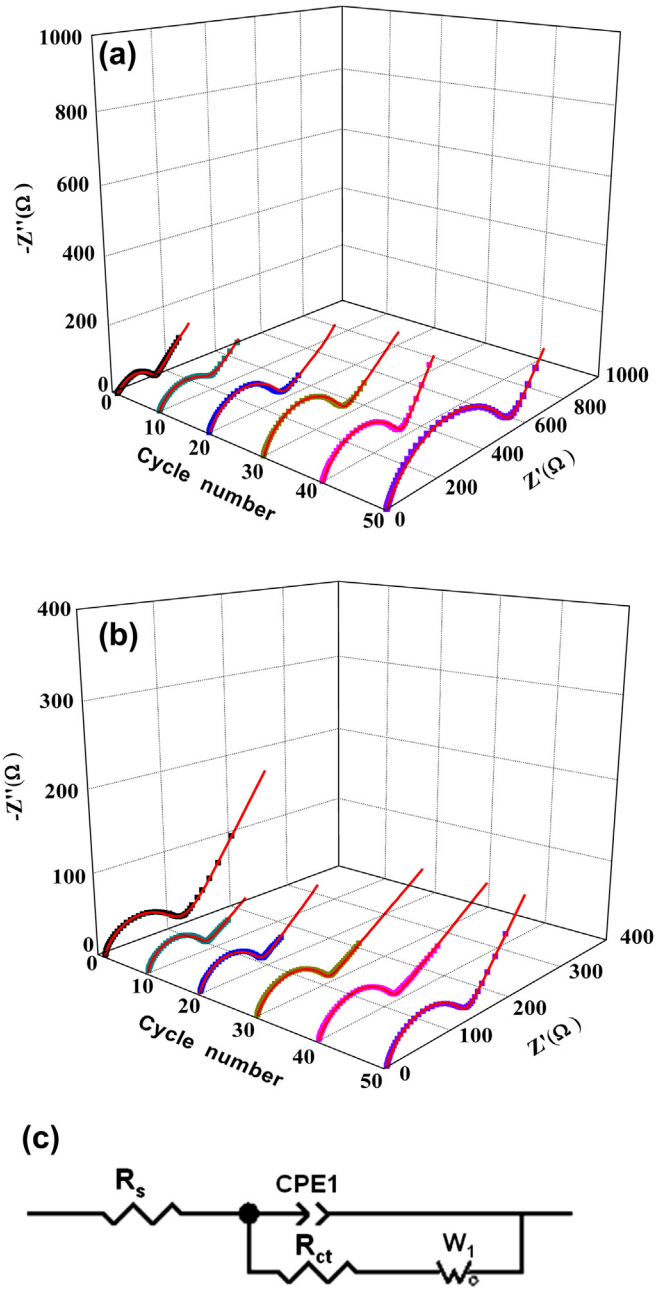

Fig. 9. Three-dimensional Nyquist plots measured for LiV_3O_8 (a) and 15 wt.% LiV_3O_8/PTh composite (b) after cycling for different cycles at 1 C; the equivalent circuit model (c).

vibration [31–33]. For PTh, the characteristic band at 3450 cm^{-1} is attributed to the O–H stretching vibration, whereas the band at 1640 cm^{-1} is normally ascribed to the O–H bending vibration from crystal or adsorbed water molecules [34]. The band located around 1384 cm^{-1} can be ascribed to C=C symmetrical stretching vibrations of the thiophene ring [35]. The band at 1112 cm^{-1} is characteristic of C_α–C_α vibrations or in-plane C–H aromatic bending vibrations [35,36]. The C_α–C_α conjunction polymer has good conductivity upon the maximum overlap of the C–C interring carbon p_z orbitals [37,38]. The band at 1031 and 783 cm^{-1} indicated a C_{ss}-H out-of-phase bending vibration and an in-phase bending vibration [39]. Vibrations between 950 cm^{-1} and 1450 cm^{-1} originate from stretching or bending bands of PTh [35,36]. The FT–IR spectrum of 15 wt.% LiV_3O_8/PTh composite is much different from that of bare LiV_3O_8. It is obvious that besides the characteristic absorption bands of LiV_3O_8, 15 wt.% LiV_3O_8/PTh composite shows characteristic absorption bands of PTh at about 3450, 1640, 1384 and 1031 cm^{-1}. The FT–IR spectrum of 10 wt.% PTh–LiV_3O_8 composite and 20 wt.% PTh–LiV_3O_8 composite (see Fig. S3) are similar to 15 wt.% LiV_3O_8/PTh composite.

Table 1
R_s and R_{ct} values of LiV_3O_8 and 15 wt.% LiV_3O_8/PTh composite after different cycles.

	R_s (Ω)						R_{ct} (Ω)					
	1st	10th	20th	30th	40th	50th	1st	10th	20th	30th	40th	50th
LiV_3O_8	4.427	4.575	4.650	4.802	5.094	5.245	137.6	188.2	267.4	280.2	290.5	495.6
15 wt.% LiV_3O_8/PTh	2.979	2.992	3.013	3.157	3.204	3.317	58.58	76.81	84.09	98.8	106.5	124.9

The particle size and morphology of the bare LiV_3O_8 and 15 wt.% LiV_3O_8/PTh composite were characterized by SEM and TEM in Fig. 6. Bare LiV_3O_8 shows a nonuniform morphology, comprising of differently sized secondary particles from 1 to 10 μm with a rough surface (see Fig. 6a). The secondary particles are composed of many primary particles with nanofibers morphology (see Fig. 6b), which are beneficial for lithium ion intercalation. HRTEM image (Fig. 6c) taken on an individual nanofiber displays clear crystal lattices with *d*-spacing of 0.220 nm, corresponding to (−301/−205) planes of monoclinic LiV_3O_8. The selected area electron diffraction (SAED) pattern shown in Fig. 6d indicates that the nanofiber is monoclinic LiV_3O_8, which is in good agreement with the XRD results shown in

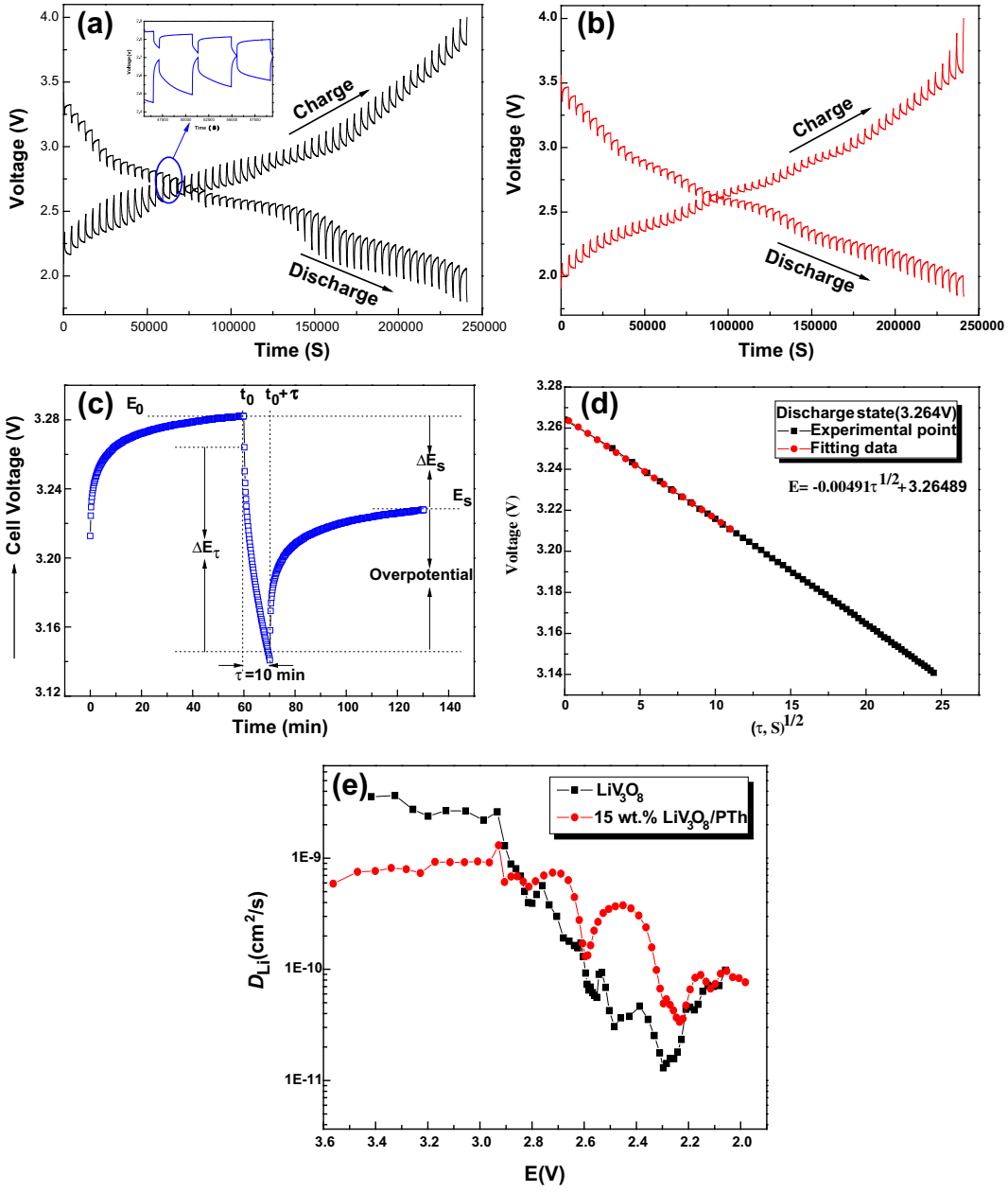

Fig. 10. The discharge/charge GITT curves of LiV_3O_8 (a) and 15 wt.% LiV_3O_8/PTh composite (b) as a function of time in the potential range of 1.8–4.0 V; *E* vs *t* profile of LiV_3O_8/PTh electrode for a single GITT during discharge process at 3.28 V with schematic representation of different profile parameters (c); linear behavior of the transient voltage changes (*E*) vs ($\tau^{1/2}$) during a single titration process of 15 wt.% LiV_3O_8/PTh electrode (d); the calculated D_{Li} from the GITT data for LiV_3O_8 and 15 wt.% LiV_3O_8/PTh composite as a function of potential during discharge process (e).

Fig. 4. The SAED pattern shown in Fig. 6h displays three ring patterns related to the (−111), (−301/−205) and (020) planes, corresponding to monoclinic LiV_3O_8. Fig. 6e and f (and Fig. S4 in Supporting Information) indicates that the particles of LiV_3O_8/PTh composites are smaller and much different from bare LiV_3O_8. This is may be due to the Fe^{3+} on the outer surface of LiV_3O_8 particle would oxidize the thiophene to initiate it's polymerization, thus forming a red-brown PTh shell (with a thickness of 3–5 nm covered on the surface of LiV_3O_8) to restrict the aggregation of LiV_3O_8 particle, which is beneficial for lithium ion diffusion (see Fig. 6f and g). Besides, the uniformly distributed PTh formed a good network of electrically conductive paths among the LiV_3O_8 particles, which are closely interlinked with each other. So active LiV_3O_8 material can get electrons from all directions and be fully utilized for lithium ion insertion and extraction reactions (corresponding with Figs.1 and 2). All these above indicate that the introduction of PTh can not only enhance electron transport but also decrease the lithium ion diffusion length by restricting the aggregation of LiV_3O_8 particle.

3.2. Electrochemical analysis of LiV_3O_8/PTh composite

The lithium ion insertion and extraction properties in the LiV_3O_8/PTh composite were studied in order to examine the effectiveness of PTh in improving the electrochemical performance of LiV_3O_8 electrode. Fig. 7 shows the cycle performance and discharge/charge profiles (insets) of bare LiV_3O_8 and 15 wt.% LiV_3O_8/PTh composite. To compare with the LiV_3O_8 cathode conveniently, the specific capacity was calculated by the total mass of LiV_3O_8 and PTh of the 15 wt.% LiV_3O_8/PTh composite. LiV_3O_8 shows multiple plateaus in discharge–charge profiles, which is caused by the lithium ion insertion/extraction processes in agreement with other reports [40–43]. This is a characteristic performance of LiV_3O_8 and makes against its application in practice. Three discharge plateaus located at about 2.8, 2.5 and 2.2 V (vs. Li^+/Li) can be identified as resulting from the single-phase insertion process, the two-phase transformation from $Li_3V_3O_8$ to $Li_4V_3O_8$ and the slower kinetic insertion process, respectively [41]. It is shown that the 15 wt.% LiV_3O_8/PTh exhibits smaller difference between charge and discharge potential plateaus, indicating lower electrochemical polarization. Besides, it is striking to note that 15 wt.% LiV_3O_8/PTh composite shows much better electrochemical performance than bare LiV_3O_8. As shown in Fig. 7a, bare LiV_3O_8 shows an initial discharge capacity of 248.5 mAh g^{-1} at 1 C, but the capacity rapidly decreases to 105.2 mAh g^{-1} after 50 cycles. When the current density is increased to 3 C, the initial discharge capacity sharply decreases to 87.7 mAh g^{-1}, and the capacity declines to 67.7 mAh g^{-1} after 50 cycles (see Fig. 7b). Bare LiV_3O_8 shows poor cycle stability and rate capability. PTh coating improves the electrochemical performance of LiV_3O_8 remarkably. The 15 wt.% LiV_3O_8/PTh composite shows an initial discharge capacity of 213.3 mAh g^{-1}, 200.3 mAh g^{-1} at 1 C, 3 C, and it decreases to 216.7 mAh g^{-1}, 197.9 mAh g^{-1} after 50 cycles, respectively (see Fig. 7c and d), which may be attributed to suppress the dissolution of active materials into the $LiPF_6$ electrolyte and improve the electrical conductivity of LiV_3O_8 significantly [44]. 10 wt.% PTh–LiV_3O_8 composite and 20 wt.% PTh–LiV_3O_8 composite both shows better electrochemical performance than the bare LiV_3O_8 (see Fig. S5 in Supporting Information). However, their electrochemical performance are poor than 15 wt.% PTh–LiV_3O_8 composite. It is mainly because that the polythiophene in 10 wt.% PTh–LiV_3O_8 composite is not enough to form a uniform conductive layer. In addition, the capacity of 20 wt.% PTh–LiV_3O_8 composite is lower than the other composites, which is probably due to that the coating layer is too thick to hinder lithium ion insertion and extraction. In conclusion, 15 wt.% LiV_3O_8/PTh composite performs remarkably larger discharge capacity and much superior capacity retention, suggesting the fascinating superiority of 15 wt.% LiV_3O_8/PTh composite as cathode materials for LIBs.

Fig. 8 shows Cyclic voltammetry (CV) profiles of LiV_3O_8 and 15 wt.% LiV_3O_8/PTh between 4.0 and 1.8 V at a scanning rate of 1 mV s^{-1}. Multiple anodic–cathodic peaks appear in the plots of LiV_3O_8 and 15 wt.% LiV_3O_8/PTh, which indicate multiple charge–discharge plateaus originates in typical lithium insertion and extraction steps of LiV_3O_8 [45,46]. There is a great difference between the first cycle CV curves and the rest, which indicates some structural modifications have probably taken place during the first charge and discharge operations. For bare LiV_3O_8, the intensity of the peaks decreases with cycling, indicating poor cycle stability (see Fig. 8a). In addition, the anodic peak potentials shift toward positive obviously with the increase of cycle number. However, with cycle increasing, the curves of 15 wt.% LiV_3O_8/PTh are nearly identical, indicating good reversibility (seen Fig. 8b). Fig. 8c compares the third CV cycle of LiV_3O_8 and 15 wt.% LiV_3O_8/PTh. LiV_3O_8 exhibits two oxidation peaks at 2.46 V and 3.25 V, and four reduction peaks at 2.41 V, 2.61 V, 3.31 V and 3.57 V, corresponding to the extraction and insertion of lithium ions in monoclinic LiV_3O_8 [41–43], respectively. This is corresponding to the charge–discharge profiles of LiV_3O_8 (see Fig. 7). However, for 15 wt.% LiV_3O_8/PTh, only two pairs of oxidation peaks (2.82 V and 3.00 V) and reduction peaks (2.44 V and 2.73 V) are observed, which is corresponding to the less plateaus of 15 wt.% LiV_3O_8/PTh in charge–discharge profiles (see Fig. 7), which is benefit for application in practice. Besides, as shown in Fig. 8c, the potential difference between the main cathodic peak and corresponding anodic peak of 15 wt.% LiV_3O_8/PTh is much smaller than that of bare LiV_3O_8, indicating the reversibility of 15 wt.% LiV_3O_8/PTh composite is much superior to that of bare LiV_3O_8.

Fig. 9 shows the three-dimensional Nyquist plots of LiV_3O_8 and 15 wt.% LiV_3O_8/PTh composite after different cycle number around 3.2 V. The EIS were recorded at room temperature during 1st to 50th discharge–charge cycles. The shapes of the Nyquist plots for each cycle are similar. It can be found that all of the plots are mainly composed of one semicircle in the high frequency region and sloping line in the low frequency region. The impedance spectra are fitted using the equivalent circuit model (See Fig. 9c), and the fitted impedance parameters are listed in Table 1. The fitting data are in good agreement with experimental data as shown in Fig. 9a and b. The equivalent circuit model includes R_s, a constant phase element (CPE) associated with the interfacial resistance, and the semi-circle is correlated with the lithium charge transfer resistance at the interface R_{ct}. The linear portion is designated to Warburg impedance (W_1), which is attributed to the diffusion of lithium ion into the bulk of the electrode materials. R_s includes the ionic resistance of the electrolyte, the intrinsic resistance of the active material, and the contact resistance at the interface active material/current collector. In this work, the difference of R_s is mainly due to the difference of resistance of the active material. It is clear from Table 1 that the R_s and R_{ct} of 15 wt.% LiV_3O_8/PTh composite are smaller than those of LiV_3O_8, indicating that 15 wt.% LiV_3O_8/PTh composite has higher conductivity than LiV_3O_8. The R_{ct} of LiV_3O_8 is 137.6 Ω after one cycle, and this value increases to 495.6 Ω after 50 cycles. However, the R_{ct} of 15 wt.% LiV_3O_8/PTh composite is 58.58 Ω after one cycle, and this value only increases to 117.9 Ω after 50 cycles. It is well-known that the lower increase of impedance during cycling means lower polarization, which, in turn, indicates good cycling behavior. These results are in good agreement with the charge–discharge performance shown in Fig. 7.

Insertion and extraction of lithium ion in/from cathode materials during charge–discharge process are the main electrode

reaction for LIBs. Thus, the lithium ion diffusion coefficient is one of the most important kinetic characteristics in electrode materials. Therefore, to obtain the chemical diffusion coefficient is important for research the effect of PTh in the composite. GITT technique was firstly developed by Weppner and Huggins to determine the diffusion coefficient of lithium ions (D_{Li}) in electrode active materials in Li_3Sb [47]. GITT is considered to be a reliable method to determine the diffusion coefficient of lithium ions (D_{Li}) with greater accuracy for compounds with varying composition or voltage, which has been extensively used to calculate the value of D_{Li} in electrode materials [48,49]. The first discharge/charge GITT curves of LiV_3O_8 and 15 wt.% LiV_3O_8/PTh electrodes as a function of time in the potential range of 1.8–4.0 V are shown in Fig. 10a and b. The cell was discharged with a constant current flux of 0.01 C for an interval of 10 min followed by an open circuit stand for 60 min to allow the cell voltage to relax to its steady-state value (E_s). The cell voltage can be stabilized to a value after 60 min open-circuit stand after each current flux, as seen the two partial GITT curves as inserts in Fig. 10a during both discharge and charge processes. Fig. 10c simply illustrates a single step of GITT. Fig. 10d shows an example of an E vs. $\tau^{1/2}$ plot recorded for LiV_3O_8 after application of 0.01 C current pulse. It can be seen that in the time domain from 10 to 100 s, the plot is roughly linear [50]. In the literatures using GITT techniques [47], the time range of 10–100 s is identical. The slope is taken from this linear range to calculate D_{Li}. On the basis of Fick's second law of diffusion and after a series of assumptions and simplifications, the chemical diffusion coefficients can be obtained by the following equation [47]:

$$D_{Li} = \frac{4}{\pi}\left(I_o\frac{V_m}{SFz_i}\right)^2\left(\frac{dE/dx}{dE/dt^{1/2}}\right)^2\left(t \ll L^2/D_{Li}\right) \quad (1)$$

where D_{Li} ($cm^2\ s^{-1}$) is the chemical diffusion coefficient of the mobile specie, V_m ($cm^3\ mol^{-1}$) is the molar volume of the active materials, F is the Faraday constant, I_0 (A) is the applied current, S (cm^2) is the total contact area between the electrolyte and electrodes, Z_i is the number of charge transfer, and L (cm) is the diffusion length. Based on Equation (1), the diffusion coefficients lithium ions calculated from the GITT curves as a function of potential during the first discharge process at initial open circuit cell potentials are shown in Fig. 10e. The size of the data points are within the error limit of estimation.

It is found that the D_{Li} vs potential plots show several minimal in the discharge processes, corresponding to the potential plateaus of charge/discharge curve and the CV peaks (Figs. 7 and 8). The D_{Li} values of LiV_3O_8 are in the range of 3.57×10^{-9} to $1.3 \times 10^{-11}\ cm^2\ s^{-1}$ during first discharge process for lithium ions intercalation, and the D_{Li} values of 15 wt.% LiV_3O_8/PTh composite are in the range of 1.3×10^{-9} to $3.7 \times 10^{-11}\ cm^2\ s^{-1}$ during first discharge process. These results are of the same orders of magnitude with D_{Li} values reported in the literature [29]. Though the D_{Li} of LiV_3O_8 larger than 15 wt.% LiV_3O_8/PTh above 2.9 V, the D_{Li} of LiV_3O_8 is smaller than 15 wt.% LiV_3O_8/PTh below 2.9 V. The main discharge plateau of LiV_3O_8 is below 2.9 V, so the electrochemical behavior below 2.9 V is more important for LiV_3O_8. Hence, PTh can significantly improve the lithium diffusion coefficient of LiV_3O_8, which is may be due to that the PTh coating provides a path for electrons, and smaller particles of 15 wt.% LiV_3O_8/PTh induce shorter diffusion distance of lithium ions and contribute to lithium ions diffusion. With the increase of the lithium diffusion coefficient, the polarization between the cathode particles and the electrolyte is decreased. Therefore, 15 wt.% LiV_3O_8/PTh shows much better cycle performance and rate capabilities than the bare LiV_3O_8.

4. Conclusions

In summary, 15 wt.% LiV_3O_8/PTh composite has been successfully synthesized via an in-situ oxidative polymerization method. A PTh layer with a thickness of 3–5 nm covered on the surface of LiV_3O_8 particles has been confirmed by HRTEM. The 15 wt.% LiV_3O_8/PTh composite shows much better cycling performance and rate capability compared with bare LiV_3O_8. The 15 wt.% LiV_3O_8/PTh composite shows excellent electrochemical performance. The discharge capacity of 15 wt.% LiV_3O_8/PTh composite remains as high as 197.9 mAh g^{-1} after 50 cycles at a high rate of 3 C. The excellent electrochemical performance of 15 wt.% LiV_3O_8/PTh composite can be ascribed to PTh coating, which could enhance electronic conductor, decrease the charge transfer resistance, increase the lithium diffusion coefficient, as was confirmed by CV, EIS and GITT tests. These results suggest that LiV_3O_8/PTh composite is one of promising cathode materials for LIBs.

Acknowledgments

This study was financially supported by the National Natural Science Foundation of China (grant no. 51202209), the Key Project Doctoral Fund of Ministry of Education of China (grant no. 20114301120007), China Postdoctoral Science Foundation (grant no. 20100480954), and the Hunan Provincial Natural Science Foundation of China (grant no. 11JJ4038).

Appendix A. Supplementary data

Supplementary data related to this article can be found at http://dx.doi.org/10.1016/j.jpowsour.2013.08.078.

References

[1] X. Ji, K.T. Lee, L.F. Nazar, Nat. Mater. 8 (2009) 500.
[2] Y. Wang, G.Z. Cao, Adv. Mater. 20 (2008) 2251.
[3] M.S. Whittingham, Chem. Rev. 104 (2004) 4271.
[4] G. Pistoia, M.L. Di Vona, P. Tagliatesta, Solid State Ionics 24 (1987) 103.
[5] H.Y. Xu, H. Wang, Z.Q. Song, Y.W. Wang, H. Yan, M. Yoshimura, Electrochim. Acta 49 (2004) 349.
[6] L. Liu, L. Jiao, J. Sun, Y. Zhang, M. Zhao, H. Yuan, Y. Wang, Electrochim. Acta 53 (2008) 7321.
[7] K. West, B. Zachau-Christiansen, S. Skaarup, Y. Saidi, J. Barker, I.I. Olsen, R. Pnenburg, R. Koksbang, J. Electrochem. Soc. 143 (1996) 820.
[8] C.Q. Feng, S.Y. Chew, Z.P. Guo, J.Z. Wang, H.K. Liu, J. Power Sources 174 (2007) 1095.
[9] H.M. Liu, Y.G. Wang, K.X. Wang, Y.R. Wang, H.S. Zhou, J. Power Sources 192 (2009) 668.
[10] Y.X. Gu, D.R. Chen, X.L. Jiao, F.F. Liu, J. Mater. Chem. 16 (2006) 4361.
[11] C.J. Cui, G.M. Wu, J. Shen, B. Zhou, Z.H. Zhang, H.Y. Yang, S.F. She, Electrochim. Acta 55 (2010) 2536.
[12] P. Kubiak, M. Pfanzelt, J. Geserick, U. Hormann, N. Husing, U. Kaiser, M. Wohlfahrt-Mehrens, J. Power Sources 194 (2009) 1099.
[13] S. Jouanneau, A. Salle, A. Verbaere, D. Guyomard, J. Electrochem. Soc. 152 (2005) A1660.
[14] L.F. Jiao, L. Liu, J.L. Sun, L. Yang, Y.H. Zhang, H.T. Yuan, Y.M. Wang, X.D. Zhou, J. Phys. Chem. C 112 (2008) 18249.
[15] N.H. Idris, M.M. Rahman, J.Z. Wang, Z.X. Chen, H.K. Liu, Compos. Sci. Technol. 71 (2011) 343.
[16] X.Y. Cao, L.J. Guo, J.P. Liu, L.L. Xie, Int. J. Electrochem. Sci. 6 (2011) 270.
[17] C. Li, H.P. Zhang, L.J. Fu, H. Liu, Y.P. Wu, E. Rahm, R. Holze, H.Q. Wu, Electrochim. Acta 51 (2006) 3872.
[18] S.T. Myung, K. Amine, Y.K. Sun, J. Mater. Chem. 20 (2010) 7074.
[19] F.H. Tian, L. Liu, X.Y. Wang, Z.H. Yang, M. Zhou, X.Y. Wang, Compos. Sci. Technol. 72 (2012) 344.
[20] A. Malinauskas, J. Malinauskiene, A. Ramanavicius, Nanotechnology 16 (2005) 51.
[21] S. Kuwabata, S. Masui, H. Tomiyori, H. Yoneyama, Electrochim. Acta 46 (2000) 91.
[22] K. Park, H. Song, Y. Kim, Y. Kim, S. Mho, W. Cho, I.H. Yeo, Electrochim. Acta 55 (2010) 8023.
[23] H.P. Wong, B.C. Dave, F. Leroux, J. Harreld, B. Dunn, L.F. Nazar, J. Mater. Chem. 8 (1998) 1019.
[24] H.P. Guo, L. Liu, Q.L. Wei, H.B. Shu, X.K. Yang, Z.H. Yang, M. Zhou, J.L. Tan, Z.C. Yan, X.Y. Wang, Electrochim. Acta 94 (2013) 113.

[25] G. Zhang, X. Li, H. Jia, X. Pang, H. Yang, Y. Wang, K. Ding, Int. J. Electrochem. Sci. 7 (2012) 830.
[26] Y. Bai, P. Qiu, Z. Wen, S. Han, J. Alloy. Compd. 508 (2010) 1.
[27] P. Novák, K. Müller, S.V. Santhanam, O. Hass, Chem. Rev. 97 (1997) 207.
[28] N. Ballav, M. Biswas, Polym. Int. 52 (2003) 179.
[29] K. Kuwabara, M. Itoh, K. Sugiyama, Solid State Ionics 20 (1986) 135.
[30] K. Nakamura, D. Nishioka, Y. Michihiro, M. Vijayakumar, S. Selvasekarapandian, T. Kanashiro, Solid State Ionics 177 (2006) 129.
[31] G. Yang, W. Hou, Z. Sun, Q. Yan, J. Mater. Chem. 15 (2005) 1369.
[32] E.P. Kovalchuk, O.V. Reshetnyak, Y.S. Kovalyshyn, J. Blazejowski, J. Power Sources 107 (2002) 61.
[33] N.V. Kosova, V.F. Anufrienko, N.T. Vasenin, S.V. Vosel, E.T. Devyatkina, J. Solid State Chem. 163 (2002) 421.
[34] Y.G. Wang, W. Wu, L. Cheng, P. He, C.X. Wang, Y.Y. Xia, Adv. Mater. 20 (2008) 2166.
[35] X.G. Li, J. Li, M.R. Huang, Chem. Eur. J. 15 (2009) 6446.
[36] H.M. Wang, G.Q. Tang, S.S. Jin, C.X. Bian, F.F. Han, D. Liang, X.C. Xu, Acta Chim. Sin. 65 (2007) 2454.
[37] J. Roncali, Chem. Rev. 92 (1992) 711.
[38] E.A. Bazzaoui, G. Levi, S. Aeiyach, J. Aubard, J.P. Marsault, P.C. Lacaze, J. Phys. Chem. 99 (1995) 6628.
[39] F. Wu, J.Z. Chen, R.J. Chen, S.X. Wu, L. Li, S. Chen, T. Zhao, J. Phys. Chem. C 115 (2011) 6057.
[40] J.Q. Xu, H.L. Zhang, T. Zhang, Q.Y. Pan, Y.H. Gui, J. Alloys Compd. 467 (2009) 327.
[41] J. Kawakita, T. Kato, Y. Katayama, T. Miura, T. Kishi, J. Power Sources 81 (1999) 448.
[42] Q.Y. Liu, H.W. Liu, X.W. Zhou, C.J. Cong, K.L. Zhang, Solid State Ionics 176 (2005) 1549.
[43] L.L. Xie, L.Q. You, X.Y. Cao, C.F. Zhang, D.W. Song, L.B. Qu, Electron. Mater. Lett. 8 (2012) 411.
[44] A.D. Pasquier, F. Orsini, A.S. Gozdz, J.M. Tarascon, J. Power Sources 81 (1999) 607.
[45] J. Kawakita, K. Makino, Y. Katayama, T. Miura, T. Kishi, Solid State Ionics 99 (1997) 165.
[46] A.S. Yu, N. Kumagai, Z.L. Liu, J.Y. Lee, J. Power Sources 74 (1998) 117.
[47] W. Weppner, R.A. Huggins, J. Electrochem. Soc. 124 (1977) 1569.
[48] K.M. Shaju, G.V. Subba Rao, B.V.R. Chowdari, Electrochim. Acta 48 (2003) 1505.
[49] K. Tang, X.Q. Yu, J.P. Sun, H. Li, X.J. Huang, Electrochim. Acta 56 (2011) 4869.
[50] M. Zhou, L. Liu, L.H. Yi, Z.H. Yang, S. Mao, Y.N. Zhou, T.T. Hu, Y. Yang, B.W. Shen, X.Y. Wang, J. Power Sources 234 (2013) 292.